

# Seismogenic fault and topography control on the spatial patterns of landslides triggered by the 2017 Jiuzhaigou earthquake

WU Chun-hao<sup>1,2</sup>  <http://orcid.org/0000-0003-3660-7747>; e-mail: 92126wch@163.com

CUI Peng<sup>1,3\*</sup>  <http://orcid.org/0000-0002-3973-5966>;  e-mail: pengcui@imde.ac.cn

LI Yu-sheng<sup>4</sup>  <http://orcid.org/0000-0002-6953-6239>; e-mail: liyusheng@cdut.cn

IRASEMA Alcántara AYALA<sup>5</sup>  <http://orcid.org/0000-0003-0794-1201>; e-mail: irasema@igg.unam.mx

HUANG Chao<sup>4</sup>  <http://orcid.org/0000-0001-8775-3192>; e-mail: huangchao10@foxmail.com

YI Shu-jian<sup>4</sup>  <http://orcid.org/0000-0002-5689-853X>; e-mail: yishujian24@foxmail.com

\* Corresponding author

<sup>1</sup> Key Laboratory of Mountain Surface Process and Hazards, Institute of Mountain Hazards and Environment, Chinese Academy of Science, Chengdu 610041, China

<sup>2</sup> University of Chinese Academy of Science, Beijing 100049, China

<sup>3</sup> Center for Excellence in Tibetan Plateau Earth Sciences, Chinese Academy of Sciences Beijing 100101, China

<sup>4</sup> State Key Laboratory of Geohazard Prevention and Geoenvironment Protection, Chengdu University of Technology, Chengdu 610059, China

<sup>5</sup> Universidad Nacional Autónoma de México, Instituto de Geografía Circuito Exterior s/n, Ciudad Universitaria, México, D.F., Distrito Federal, MX 04510

**Citation:** Wu CH, Cui P, Li YS, et al. (2018) Seismogenic fault and topography control on the spatial patterns of landslides triggered by the 2017 Jiuzhaigou earthquake. Journal of Mountain Science 15(4). <https://doi.org/10.1007/s11629-017-4761-9>

© Science Press, Institute of Mountain Hazards and Environment, CAS and Springer-Verlag GmbH Germany, part of Springer Nature 2018

**Abstract:** Jiuzhaigou National Park, located in northwest plateau of Sichuan Province, is a UNESCO World Heritage Site, and one of the most popular scenic areas in China. On August 8, 2017, a  $M_w$  6.5 earthquake occurred 5 km to the west of a major scenic area, causing 25 deaths and injuring 525, and the Park was seriously affected. The objective of this study was to explore the controls of seismogenic fault and topographic factors on the spatial patterns of these landslides. Immediately after the main shock, field survey, remote-sensing investigations, and statistical and spatial analysis were undertaken. At least 2212 earthquake-triggered landslides were identified, covering a total area of 11.8 km<sup>2</sup>. These

were mainly shallow landslides and rock falls. Results demonstrated that landslides exhibited a close spatial correlation with seismogenic faults. More than 85% of the landslides occurred at 2200 to 3700 m elevations. The largest quantity of landslides was recorded in places with local topographic reliefs ranging from 200 to 500 m. Slopes in the range of ~20°–50° are the most susceptible to failure. Landslides occurred mostly on slopes facing east-northeast (ENE), east (E), east-southeast (ESE), and southeast (SE), which were nearly vertical to the orientation of the seismogenic fault slip. The back-slope direction and thin ridge amplification effects were documented. These results provide insights on the control of the spatial pattern of earthquake-triggered landslides modified by the synergetic effect of seismogenic faults and topography.

**Received:** 15 November 2017

**Revised:** 28 December 2017

**Accepted:** 15 January 2018

**Keywords:** 2017 Jiuzhaigou earthquake; Landslide; Seismogenic fault; Topography; Spatial pattern

## Introduction

The Jiuzhaigou earthquake occurred at 21:19 on 8th August 2017 (Beijing time UTC+8). A magnitude of  $M_s$  7.0 was reported by the China Earthquake Networks Center (CENC), and a  $M_w$  6.5 was reported by the U.S. Geological Survey (USGS). The earthquake hypocenter was located at 33.20°N, 103.82°E, at a 12 km depth, as determined by CENC, and at 33.193°N, 103.855°E, at a 9 km depth, as determined by USGS. According to the China Earthquake Administration, as of 20:00 (Beijing time UTC+8) on August 13th, the earthquake caused 25 deaths, and injured 525 people. A total of 73,617 buildings were damaged (76 buildings collapsed), and a total of 176,492 people were affected (including tourists in the park).

The Jiuzhaigou National Park has been listed as the UNESCO World Heritage Site since 1992 and has been considered as one of the most popular scenic area for Chinese residents and tourists. It is excellent for viewing multilevel waterfalls, dozens of turquoise-colored lakes, and attractive red, yellow and orange forests. However, the Park suffered severe damage from the Jiuzhaigou earthquake. Many park roads were destroyed by landslides, and the park was forced to close. This event focused public attention at national and international level regarding post-earthquake World Heritage Site recovery and disaster risk awareness and preparedness in mountain areas. As post-earthquake reconstruction planning continues, the documentation of the spatial distribution of landslides and their associated dynamics has provided guidance for the selection of safer places to reconstruct.

As in previous seismic events, including the 1994 Northridge  $M_w$  6.7 earthquake (Stein et al. 1994), 2010 Haiti  $M_w$  7.0 earthquake (Hayes et al. 2010), 2013 Lushan  $M_w$  6.6 earthquake (Xu et al. 2013) and 2014 Ludian  $M_w$  6.1 earthquake (Chen et al. 2015), the 2017 Jiuzhaigou  $M_w$  6.5 earthquake was also a buried-rupture earthquake (Xu et al. 2017; Ji et al. 2017). When detailed surface rupture information is lacking, the unique correlation

between spatial patterns of earthquake-triggered landslides and rupture processes can provide insight (Meunier et al. 2013; Xu et al. 2014; Zhou et al. 2016). These studies have provided empirical evidences to understand the relationship between seismogenic faults and landslides. Earthquake-triggered landslides are surface processes, which were also affected by topography (Korup et al. 2007; Gorum et al. 2013; Chen and Cui 2017). Topographic factors such as elevation, local topographic relief, slope gradient, and slope aspect are used to analyze the controlling effect of topography (Cui et al. 2014; Kargel et al. 2015). Since earthquake-triggered landslides are a complex phenomenon, other factors also influence their spatial distribution. For example, there is a high statistical correlation between coseismic landslides and the estimated severity of ground shaking and specially Arias Intensity (Harp and Wilson 1995; Hsieh and Lee 2011; Chousianitis et al. 2014). Lithology and potential site-amplification phenomena (Harp and Jibson 2002; Meunier et al. 2008), hydrological conditions (Kieffer et al. 2006; Cui et al. 2017a; Cui et al. 2017b), and even the season of earthquake occurrence can affect spatial distribution and change slope failure scenarios (Chousianitis et al. 2016). Among the several factors that impact the distribution of earthquake-triggered landslides, the present investigation is only studied seismogenic faults and topography. Therefore, the study focused on how the interaction of faulting and topography influences landslide occurrence. It was essential to combine these two critical factors for landslide distribution analysis, to provide stability evaluations of seismic hazard areas, and help to identify areas of potential damage due to faulting processes.

A field survey of seismogenic faults and coseismic landslides in the area affected by the earthquake was undertaken immediately after the main shock. Additionally, a remote-sensing investigation of earthquake-triggered landslides was also carried out. This paper attempts to explore seismogenic fault and topographic controls on the spatial pattern of landslides triggered by the 2017 Jiuzhaigou earthquake. To achieve this aim, a substantially complete inventory of 2212 coseismic landslides was compiled, followed by a preliminarily analysis of the relationships among

these coseismic landslides, seismogenic faults and topographic factors. The topographic effects of back-slope direction and thin ridge amplification effects were also introduced. Finally, this paper summarized the synergetic effect of seismogenic faults and topography to further understand the spatial characteristics of earthquake-triggered landslides, and the significance of establishing an integrated strategy of disaster risk awareness and preparedness for the inhabitants and visitors.

## 1 Study Area

This study focused on the main epicentral area of the 2017 Jiuzhaigou earthquake. It is located in

the south western portion of the Qinling fold system and the northern part of the Longmenshan thrust belt. This area belongs to the Bayankala block of eastern Tibet Plateau (Figure 1). Since 1876, five earthquakes of  $M_s \geq 7.0$  and 15 earthquakes of  $M_s \geq 6.0$  have been recorded in this region (Li et al. 2017). The epicenter of the 2017 Jiuzhaigou earthquake was located on the Danzu valley about 5 km to the west of the main scenic spot of the Jiuzhaigou National Park. A rectangular shaped area around the epicenter was chosen for this study. This was between  $33.08^{\circ}\text{N}$  and  $33.38^{\circ}\text{N}$ ,  $103.68^{\circ}\text{E}$  and  $103.95^{\circ}\text{E}$  (Figure 2). The main faults trend to the north-west throughout most of the region, but also there are North-trending and Northeast-trending faults. The existence of the

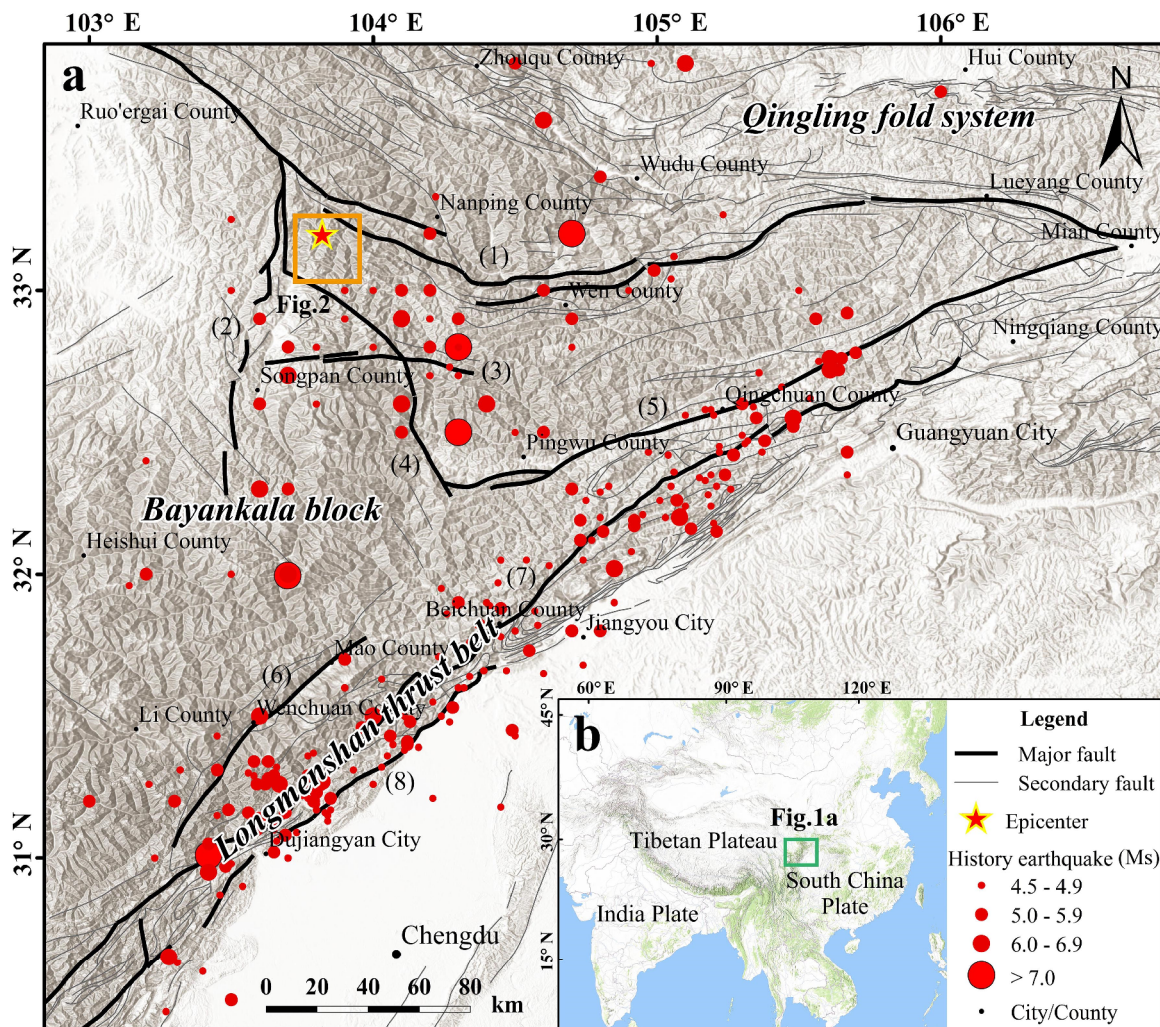


**Figure 1** Tectonic setting of northeastern margin of the Tibetan Plateau (a) and the location of the area (b). Red star is the location of the epicenter of the  $M_w 6.5$  August 2017 Jiuzhaigou earthquake. Faults names: (1): Wenxian-Maqu fault zone; (2) Minjiang fault; (3) Xueshan fault; (4) Huya fault; (5) Qingchuan-Pingwu fault; (6) Wenchuan-Maoxian fault; (7) Yingxiu-Beichuan fault; (8) Guankou-Anxian fault.

seismogenic fault of the earthquake was controversial since there was no obvious evident about surface rupture (Li et al. 2017; Xu et al. 2017; Ji et al. 2017). In previous research (Li et al. 2017), and prior to the interpretation of landslides (Dai et al. 2017), several research methods including field investigations, radon activity tests, remote sensing images, focal mechanism solution, and rupture process results were used. Two surface rupture zones trending West-Northwest were identified and are believed to be the ground coseismic ruptures caused by blind strike-slip seismogenic faults (Figure 2). Other studies support the general trends of the seismogenic fault geometry (Ren et al. 2017; Zhang et al. 2017). Analysis of the relationship between seismic faults and coseismic landslides presented in this paper is based on the above conclusion.

There are two main directions (NNW-trending and NNE-trending) of high mountains and valleys. Along these, tectonic uplift, river incision, and glaciation have resulted in significant elevation difference and varied landforms. Elevations in this region range from 2180 to 4640 meters above sea level (m asl) with slope gradients of  $\sim 2.3^\circ$ - $74.8^\circ$ . Terrain in the southwest and the central sectors is relatively high, whereas in the northeast it is relatively low. The Bai, Jiuzhai, and Rize rivers and many other watercourses occur in the region. The study area is situated in a subtropical semi-humid area. Mean annual precipitation is about 761.8 mm and mean annual temperature is of  $7.3^\circ\text{C}$  during the year (Cui et al. 2005). The vegetation cover of the area above 3700 m asl

is sparse (Figure 2) due to frost weathering and permanent snow.

## 2 Materials and Methods

Analysis of the spatial patterns of coseismic landslides and the evaluation of landslide hazards requires the development of a reliable inventory map of the coseismic landslides. This inventory map was obtained by combining visual interpretation of multi-scale remote sensing images and field investigation. The pre-earthquake images were high-resolution Google Earth images

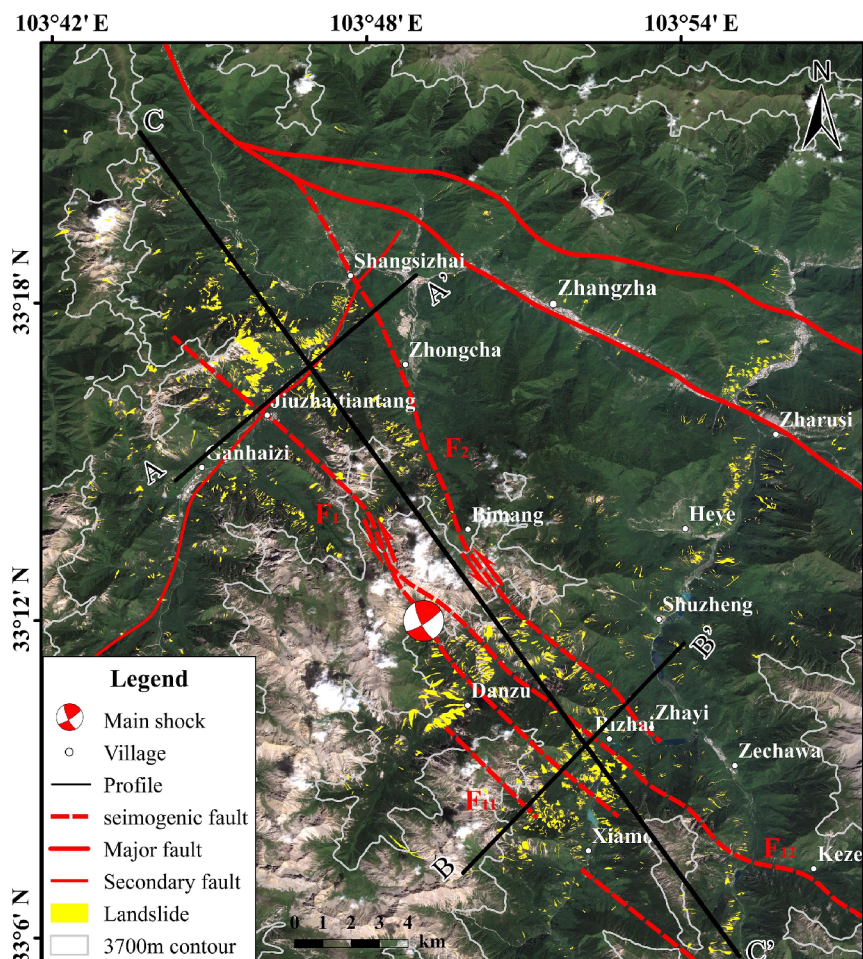


**Figure 2** Earthquake-triggered landslide inventory map (The complementary interpretation work of this study was based on the first-published results by Dai et al. (2017) and regional tectonic setting of the 2017 Jiuzhaigou earthquake. Red dash lines are seismogenic faults modified from Li et al. (2017). F<sub>1</sub> (F<sub>11</sub> and F<sub>12</sub>) are branch faults of F<sub>1</sub> and F<sub>2</sub> are the numbers of seismogenic faults. A-A', B-B', and C-C' are profiles for subsequent analysis. Beach ball shows focal mechanism by China Earthquake Networks Center. The base map is a Sentinel-2 image downloaded from USGS (<http://glovis.usgs.gov/>)).

(7th December 2015 and 13th August 2013). Post-earthquake multispectral images included 1 m high-resolution aerial imagery (11th August 2017, provided by the Geometrics Center of Sichuan province, China), Gaofen-2 (9th August 2017, 4 m resolution, provided by China Centre for Resources Satellite Data and Application) and Sentinel-2 images (6th September 2017, 10 m resolution, downloaded from USGS, <http://glovis.usgs.gov/>). The available imagery data covered a great extent of the region affected by the earthquake. Coseismic landslides were visually identified by comparing pre- and post-earthquake images using ArcGIS 9.3 to avoid mixing pre-earthquake landslides. Bare rock and landslide deposits can be easily identified in images by identifying their bright contrast against vegetation areas. This characteristic was used as a distinguishing mark for the visual interpretation of landslides. Polygons were used to represent landslides so that the location and planar area of each landslide and the total number of landslides could be estimated. The interpretation work of this study was based on the results of Dai et al. (2017), which were complemented with hundreds of additional landslides in the area using extra imagery. Likewise, about 10% of the landslides from preliminary interpretation were verified in the field on foot or using a mini quadrotor UAV.

To perform spatial distribution analysis to correlate coseismic landslides with topography, ASTER Global Digital Elevation Model Version 2 (ASTER GDEM-2) with a pixel resolution of 30 m was used. The topographic factors including elevation, local topographic relief, slope gradient, and slope aspect were derived from ASTER GDEM-2. Three different proportions were calculated as indexes to quantify the correlations between landslides and topographic factors:  $P_s$ ,  $P_a$  and  $P_n$ .  $P_s$  is the proportion of planar area of a factor class to the whole study area.  $P_a$  is the proportion of the landslide planar area within a factor class to the whole landslide-occupying area.  $P_n$  is the proportion of the landslide number within a factor class to the total landslide number. By comparing  $P_s$ ,  $P_a$  and  $P_n$  of different factor class in radar maps, knowledge related to topographic effects can be obtained. To detect general patterns and distinct clusters of landslides, three profiles and two unique areas were chosen and comparisons were made

regarding the spatial distribution of landslides density (landslide number and landslide area).

### 3 Results

#### 3.1 Regional landslide distribution

The 2017 Jiuzhaigou earthquake triggered at least 2212 landslides within an area of ~1275 km<sup>2</sup>, and up to a distance of ~26 km from the epicenter. These landslides covered a superficial area of 11.8 km<sup>2</sup> and the minimum, maximum, and mean areas of these landslides were estimated as of 9.7 m<sup>2</sup>, 231,297.3 m<sup>2</sup>, and 5312.9 m<sup>2</sup>, respectively. Figure 2 shows the spatial distribution of the coseismic landslides. The planar area of the largest 17 landslides is greater than 50,000 m<sup>2</sup>, accounting for 11% of the entire landslide area. This result suggests small scale landslides contributed relatively more to the whole coseismic landslides. The dependence of landslide probability densities ( $p$ ) on landslide area ( $A_L$ ) is given in Figure 3. The landslide inventory of the Jiuzhaigou earthquake is nearly complete and it shows a characteristic inverse-gamma distribution (a ‘roll-over’ shape for small landslides and a power-law shape for medium and large landslides). The graph also indicates that small scale landslides are dominant

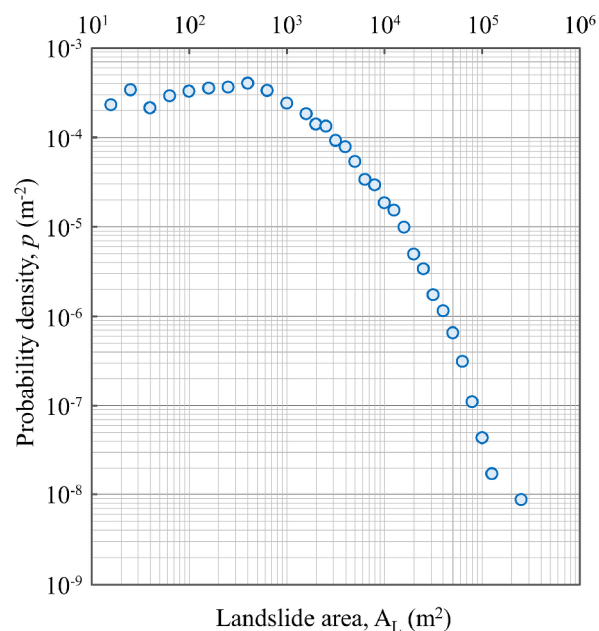


**Figure 3** Probability density of log-binned landslide planar area for the 2017 Jiuzhaigou earthquake.

(Malamud et al. 2004; Guzzetti et al. 2009). Field investigations studies also found that shallow landslides were the most common type, followed by rock falls, debris slides, and wedge failures (Figure 4).

### 3.2 Correlation between coseismic landslides and seismogenic faults geometry

Crossing the seismogenic faults, two profiles (A-A' and B-B') in Figure 2 were selected to implement statistics of the spatial pattern and seismogenic fault geometry of the landslides. The landslide area and number of each band with 500 m width and 1.1 km length are illustrated in Figure 5-6, and the band number starts from southwest to northeast. Within and outside of the corridor confined by seismogenic faults, the landslide density shows a conspicuous large gap. The data also reveal that the number and the area of landslides decrease with increasing distance from the seismogenic faults. These figures show an obvious correlation between the geometry of seismogenic faults and the coseismic landslides. In general, landslides triggered by an earthquake with a strike-slip focal mechanism are usually concentrated along the fault trace or form a narrow

corridor close to the seismogenic faults, such as the 2002 Denali earthquake (Gorum et al. 2014) and the 2010 Yushu earthquake (Xu and Xu 2014).

### 3.3 Correlation between coseismic landslides and topographic factors

#### 3.3.1 Elevation

Elevation plays an important role in landslide distribution due to its association with land cover, roads and river valleys, slope material, and the seismic wave amplification effect. A contour map of 300 m intervals and statistical calculation are given in Figure 7a and Table 1. Approximately 85% of landslides occurred at elevations of ~2200-3700 m asl with a corresponding elevation class area of 54.7%. A great number of small-scale landslides, at ~2200-2500 m asl occurred near rivers and roads which provided suitable conditions for landslide development. Of interest is that the elevation class area above 3700 m asl occupies 22.5%, while the landslide area of this class only occupies 4.8%. The area above 3700 m asl is mainly controlled by strong frost weathering so there are few slopes at critical states that are easily triggered by earthquakes. Also, the average slope angle ( $27.1^\circ$ ) and local topographic relief (333.7m) of this area is smaller than in the area where most landslides

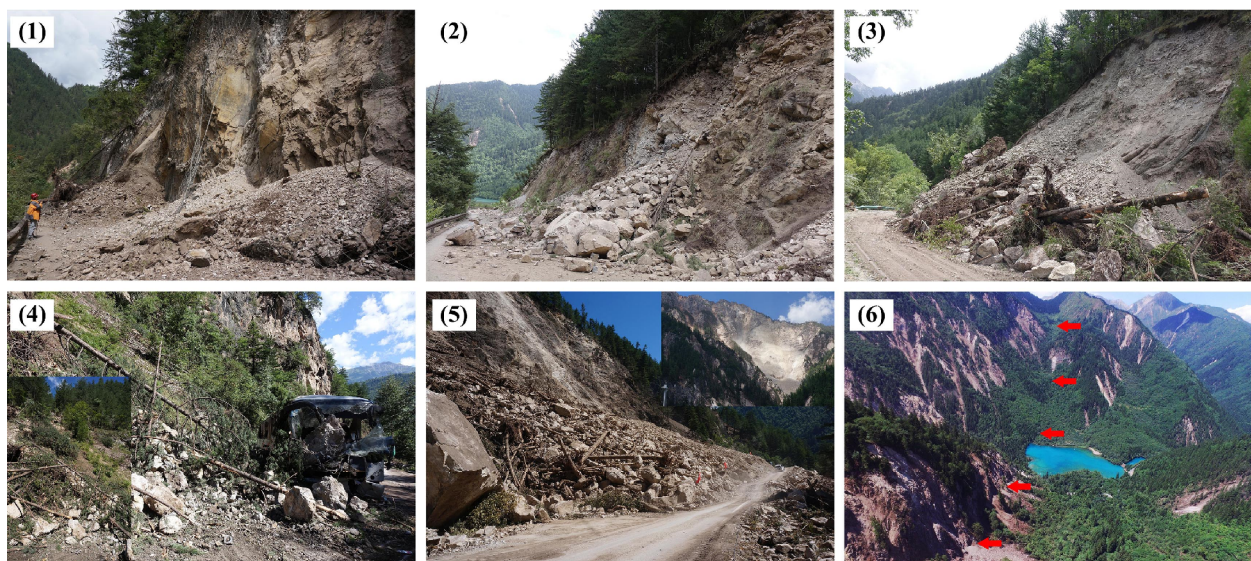


**Figure 4** Typical field photos of landslides triggered by 2017 Jiuzhaigou earthquake. (1)-(3) Wedge failures, fractured rock slides, and a colluvium slide along the roads in the Jiuzhaigou National Park, respectively; (4) Rock falls smashed a car and injured some people in the car near Shangsizhai; (5) The largest landslide (rock avalanche) triggered by 2017 Jiuzhaigou earthquake near Jiuzhaitiantang; (6) Unmanned aerial vehicle photo of some shallow landslides and rock falls near Rizhai in the Jiuzhaigou National Park. The red arrows point out the  $F_{12}$  seismogenic fault trace aforementioned in Figure 2.

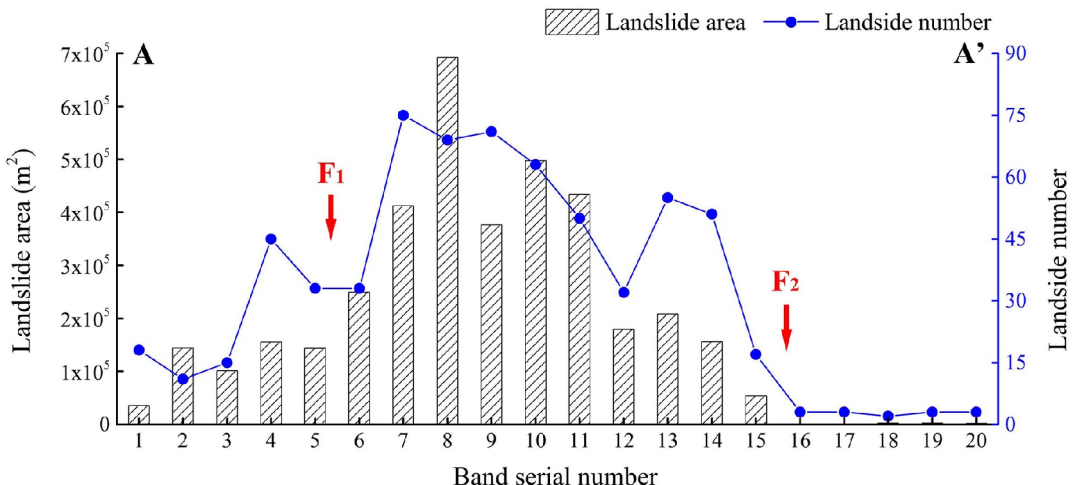


**Figure 5** Correlation between landslide density and seismogenic faults of A-A' profile (Figure 2).

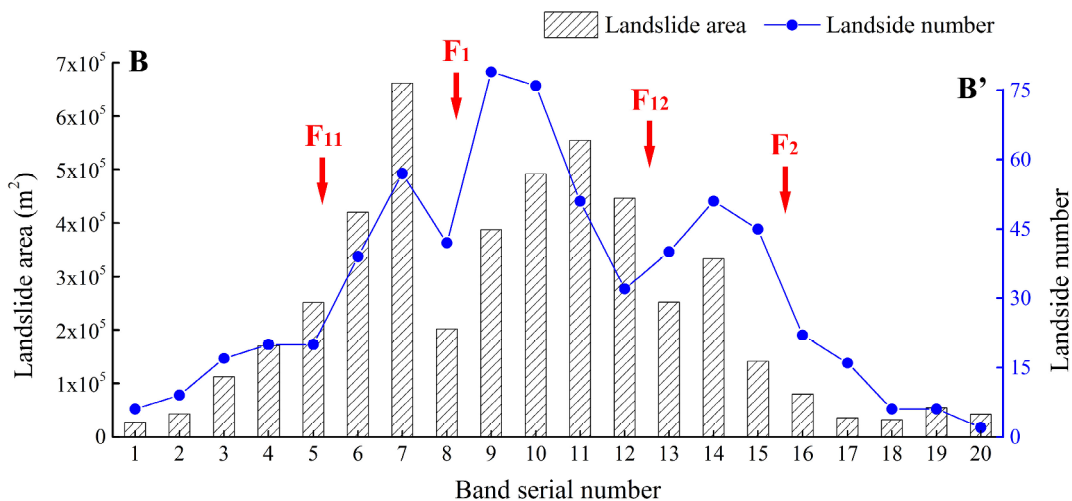


**Figure 6** Correlation between landslide density and seismogenic faults of B-B' profile (Figure 2).

were concentrated (the average slope angle was  $34.1^\circ$  and local topographic relief was 384.8m).

### 3.3.2 Local topographic relief

Local topographic relief is the difference between local maximum elevation and local base level (Korup et al. 2010), and represents the relative gravitational potential energy of a slope. Higher slopes with a particular slope angle have a greater gravitational potential energy that can be transformed into kinetic energy and therefore have a higher susceptibility to failure. Local topographic relief in the study area ranges from 0.4~830 m and was classified in intervals of 100m (Table 1). As represented in Figures 7b and 8b, topographic relief is the major landslide controlling factor in contrast to other topographic aspects. Relief

between 400 and 700 m accounts for less than 26% of the whole area, but 53% of the coseismic landslides of occurred in this sector.

### 3.3.3 Slope gradient

In general, a greater slope angle results in larger sliding force of the slope so it is more susceptible to landslide generation (Cui et al. 2013). We divided slope gradient of the region (Figure 7c) into 8 classes:  $<10^\circ$ ,  $10^\circ-<20^\circ$ ,  $20^\circ-<30^\circ$ ,  $30^\circ-<40^\circ$ ,  $40^\circ-<50^\circ$ ,  $50^\circ-<60^\circ$ ,  $60^\circ-<70^\circ$ , and  $>70^\circ$ . Statistical calculation and correlation analysis results are shown in Table 1 and Figure 8c, respectively. The study area is dominated by moderate to steep slope ( $\sim 10^\circ-40^\circ$ ) which account for 81.2% of the whole region. Landslide density was greatest on slopes of  $\sim 20^\circ-50^\circ$  including 85.5%

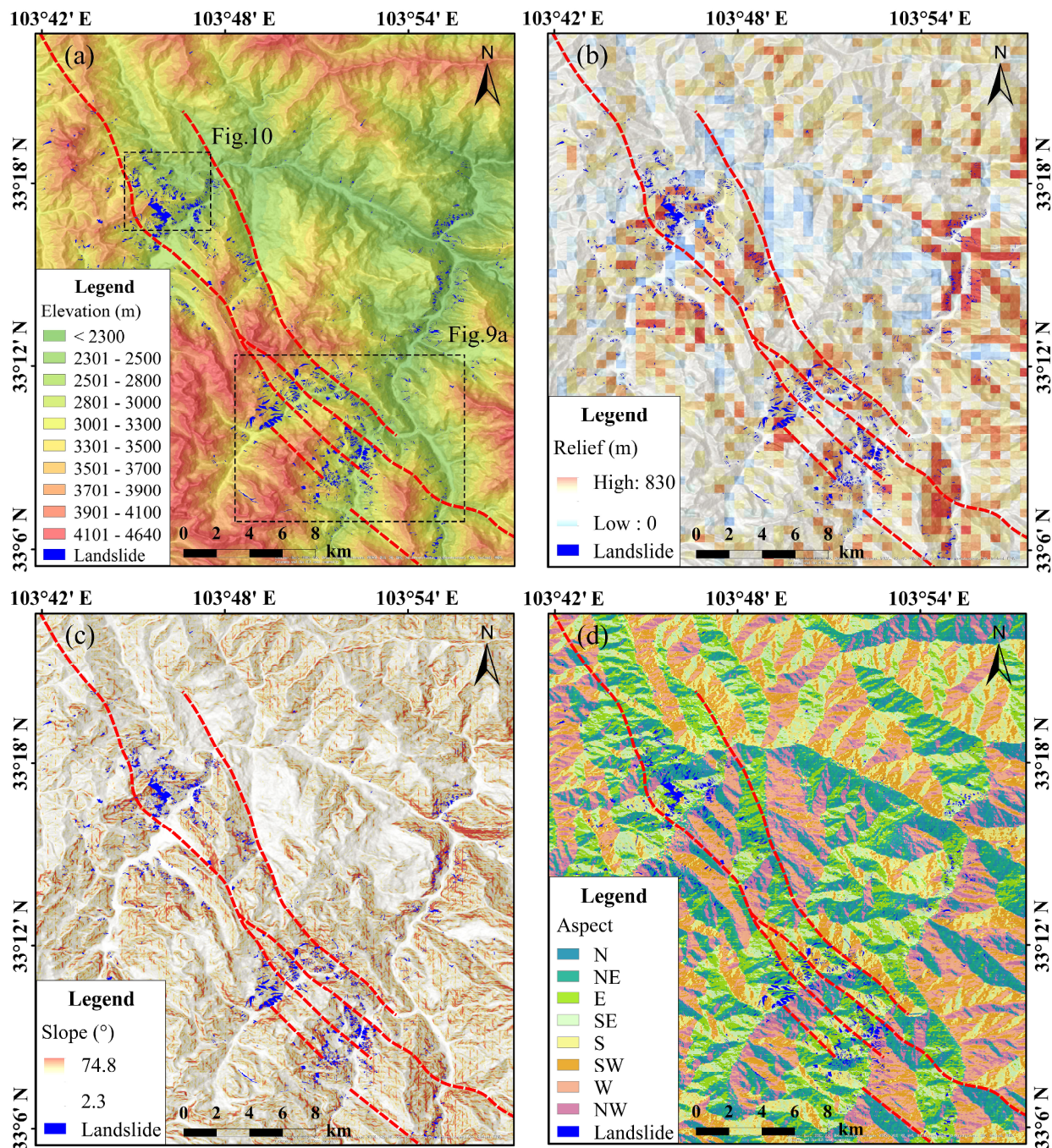


**Figure 7** Spatial distribution of landslides (blue polygons) triggered by 2017 Jiuzhaigou earthquake with topographic factors ((a) Elevation; (b) Local topographic relief; (c) Slope gradient; (d) Slope aspect). Red dash lines are seismogenic faults modified from Li et al. (2017).

of all coseismic landslides. Landslide area and number increase with slope angle up to  $40^\circ$ , and then decrease after  $40^\circ$ .

### 3.3.4 Slope aspect

Slope aspect may be the only topographic parameter with orientation in common

topographic distribution analysis, so it is usually combined with other directional parameters for further examination. Previous studies showed that slope aspect influences weathering condition, temperature, precipitation, sediment condition, and land cover and so aspect could play a role in landslide susceptibility (Yalcin 2008; Kamp et al.

**Table 1** The relationship between landslides and different topographic factors within the study area of the 2017 Jiuzhaigou earthquake

Factors	Intervals	Area (km <sup>2</sup> )	Landslides		$P_s$	$P_a$	$P_n$
			Area (km <sup>2</sup> )	Numbers			
Elevation (m asl)	< 1900	1.4	0	0	0.1	0	0
	1900–< 2200	26.5	0.2	60	2.2	1.9	2.7
	2200–< 2500	84.6	0.8	312	6.6	7.1	14.1
	2500–< 2800	150.2	2.0	475	11.8	17.1	21.5
	2800–< 3100	207.0	3.6	658	16.2	30.5	29.7
	3100–< 3400	256.1	3.2	457	20.1	26.9	20.7
	3400–< 3700	261.8	1.4	187	20.5	11.7	8.5
	3700–< 4000	181.3	0.4	51	14.2	3.8	2.3
	4000–< 4300	96.8	0.1	12	7.6	1.0	0.5
	4300–< 4496	9.3	0	0	0.7	0	0
Relief (m)	< 100	2.2	0.002	1	0.2	0.02	0.05
	100–< 200	97.3	0.1	60	7.6	1.0	2.7
	200–< 300	377.2	1.6	419	29.6	13.6	18.9
	300–< 400	466.3	3.8	802	36.5	31.8	36.3
	400–< 500	263.5	4.4	653	20.7	37.5	29.5
	500–< 600	59.4	1.6	211	4.7	13.5	9.5
	600–< 700	8.0	0.3	53	0.6	2.2	2.4
	700–< 800	0.7	0.042	12	0.1	0.4	0.5
	> 800	0.4	0.001	1	0	0.006	0.051
	<10	83.8	0.1	34	6.6	1.2	1.5
Slope (°)	10–<20	258.1	0.5	158	20.2	4.3	7.1
	20–<30	416.6	2.4	530	32.7	20.2	24.0
	30–<40	360.6	4.5	855	28.3	38.2	38.7
	40–<50	132.9	3.3	506	10.4	28.4	22.8
	50–<60	21.3	0.8	112	1.7	6.7	5.1
	60–<70	1.7	0.1	17	0.1	1.0	0.8
	> 70	0	0	0	0	0	0
	N	74.9	0.2	48	5.9	2.0	2.2
Aspect	NNE	86.2	0.8	143	6.8	6.7	6.4
	NE	95.6	0.9	193	7.5	7.8	8.7
	ENE	97.2	1.4	266	7.6	12.2	12.0
	E	98.8	1.4	292	7.7	12.0	13.2
	ESE	82.5	1.3	240	6.5	11.3	10.9
	SE	70.7	1.3	222	5.5	11.4	10.1
	SSE	58.6	0.9	165	4.6	7.5	7.5
	S	60.8	0.5	93	4.8	4.5	4.2
	SSW	67.7	0.4	59	5.3	3.4	2.7
	SW	83.8	0.4	95	6.6	3.2	4.3
	WSW	90	0.6	83	7.1	4.7	3.7
	W	91.3	0.3	78	7.2	2.5	3.5
	WNW	79.0	0.5	75	6.2	4.2	3.4
	NW	71.4	0.4	77	5.5	3.2	3.5
	NNW	66.5	0.4	83	5.2	3.4	3.7

**Notes:** Area is the planar area of a factor class to the whole study area.  $P_s$  is the proportion of planar area of a factor class to the whole study area.  $P_a$  is the proportion of the landslide planar area within a factor class to the whole landslide-occupying area.  $P_n$  is the proportion of the landslide number within a factor class to the total landslide number.

2008; Papathanassiou et al. 2013). However, this type of influence may not be applicable to landslides triggered by strong ground motion because it is closely related to seismogenic fault slip

and directional seismic wave propagation. Slope aspect of the region (Figure 7d) was divided into the following 16 classes: North (N, ~348.76°–360° and ~0–11.25°), North-Northeast (NNE, ~11.26°–33.75°), Northeast (NE, ~33.76°–56.25°), East-Northeast (ENE, ~56.26°–78.75°), East (E, ~78.76°–101.25°), Southeast (SE, ~101.26°–123.75°), East-Southeast (ESE, ~123.76°–146.25°), South-Southeast (SSE, ~146.26°–168.75°), South (S, ~168.76°–191.25°), South-Southwest (SSW, ~191.26°–213.75°), Southwest (SW, ~213.76°–236.25°), West-Southwest (WSW, ~236.26°–258.75°), West (W, ~258.76°–281.25°), West-Northwest (WNW, ~281.26°–303.75°), North west (NW, ~303.76°–326.25°), and North-Northwest (NNW, ~326.26°–348.75°). As shown in Table 1 and Figure 8d, slope aspect NEE and WSW appear to be the major directions of the study area. Nonetheless, 68.8% of all landslides corresponded to slope aspects NNE~SSE (~11.26°–168.75°) and the slope face was nearly vertical to the orientation of seismogenic fault slip. Tibaldi et al. (1995) also found that landslides were more likely to occur on slopes facing nearly vertical to strike line of seismogenic faults.

### 3.4 Topographic effects

The results are consistent with study results by Dai et al. (2017), which reported the coseismic landslides distribution

of the 2017 Jiuzhaigou earthquake exhibited a close spatial correlation with seismogenic faults. However, Figure 2 shows that, there were three major landslide concentration regions: the Danzu

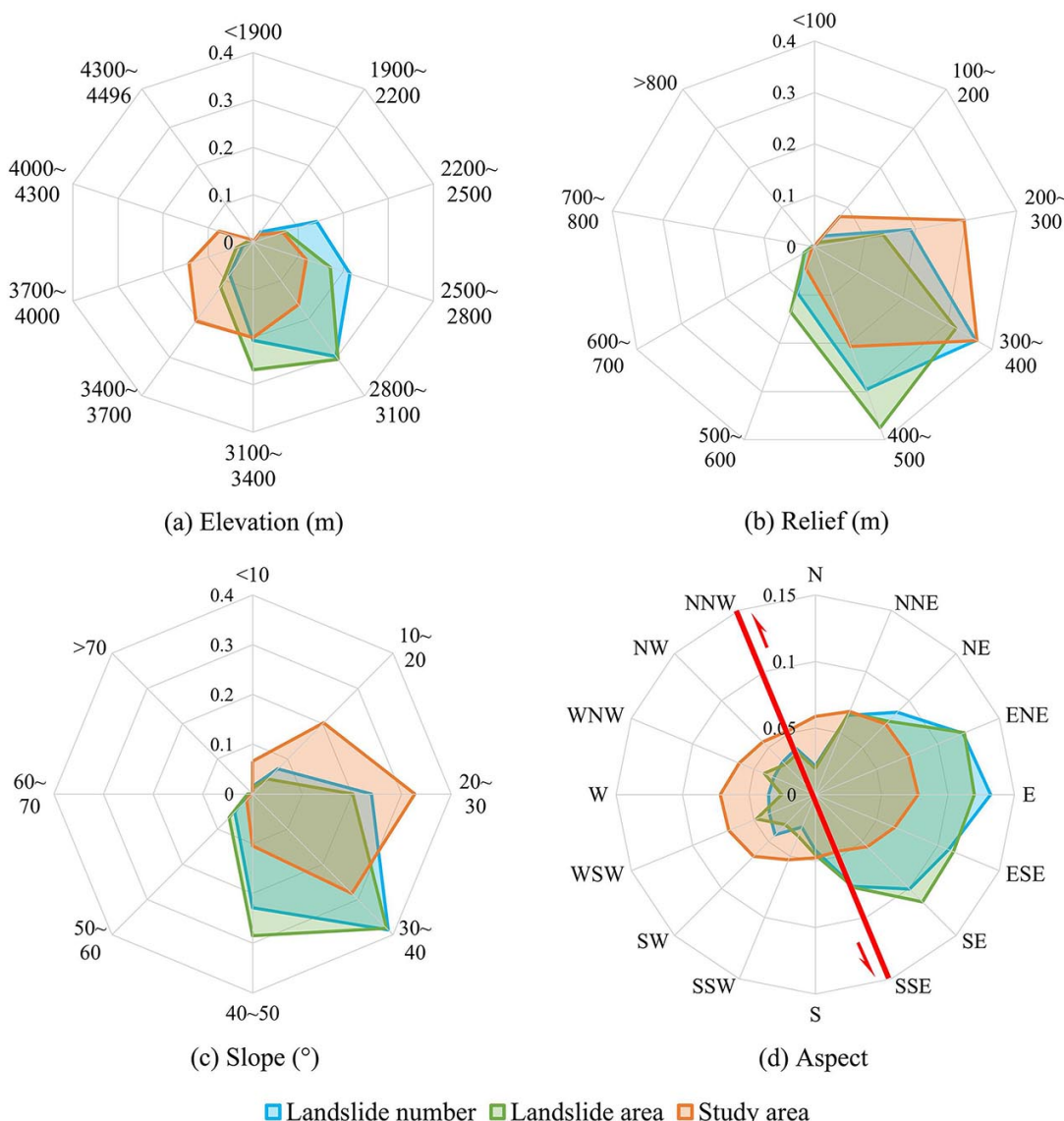


**Figure 8** Correlation between landslide density and topographic factors (a. Elevation; b. Local topographic relief; c. Slope gradient; d. Slope aspect). The red solid line from SSE-NNW in Figure 8d represents the general striking direction of seismogenic faults, and the arrows represents left lateral slip.

valley, the Rizhai valley, and the ridge near Jiuzhaitiantang. This suggests that landslide distribution cannot be entirely explained by geological structure and indicates that topographic effects should also be considered.

Back-slope direction effect was described by a study of the 2008 Wenchuan earthquake (Xu et al. 2011). It is more likely for landslides to be triggered at the rear than at the front of the slope relative to seismic wave spreading when valleys are almost perpendicular to the seismogenic faults. The probable reason is that stress changes differently due to seismic wave reflection and refraction

between the internal slope and the slope surface (Xu et al. 2011). The results from around the Danzu, Rizhai and Zechawa valley support this possibility. Figure 9a presents an area comprising the three main valleys which are nearly perpendicular to seismogenic faults. The epicenter was located at the northwestern part of Danzu valley. Thus, seismic waves spread from NW to SE throughout the entire area. According to the relative direction of seismic wave spreading, the three valleys were divided into three frontslopes and three backslopes and the landslide area density of each slope was calculated (Figure 9b). The landslide area density of the

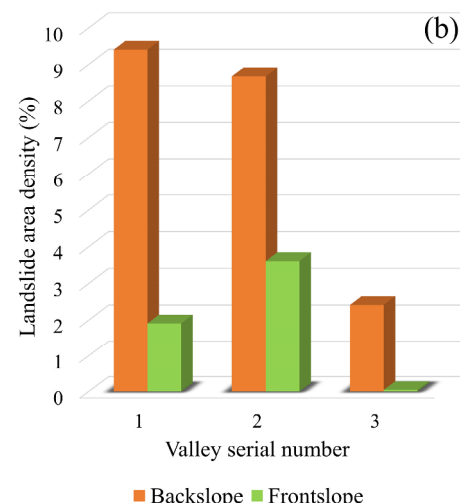
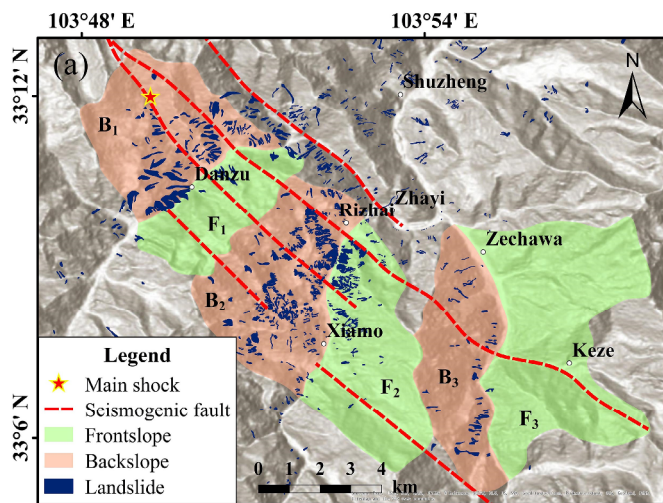


**Figure 9** (a) Earthquake-triggered landslide inventory map of direction effect area and zoning of valleys (enveloped by dash line in Figure 7a). B<sub>1</sub> and F<sub>1</sub>, B<sub>2</sub> and F<sub>2</sub>, and B<sub>3</sub> and F<sub>3</sub> are backslope and frontslope of the Danzu valley, the Rizhai Valley, and the Zechawa valley, respectively; (b) Comparison of landslide area density in the 3 valleys (Danzu valley, Rizhai valley, and Zechawa valley).

backslopes was larger than that of the frontslopes (Figure 9).

The largest landslide was near Jiuzhaitiantang (Figure 2) about 11 km northwest to the epicenter, where the thin mountain ridge has a NEE direction with slope angles of 40°~55° on its two-sided slope and a ridge height of 1200 m above the valley floor. The ridge was one of the most seriously affected areas (Figure 10). Previous studies (Davis and West, 1973; Pischutta et al. 2010; Luo et al. 2014; Poursartip et al. 2017) noted that a mountain slope ground motion topography amplification effect is obvious in the earthquake affected area and that the amplification effect on peak acceleration is more intense for the thinner ridge of a two-sided slope by numerical simulation (Zhou et al. 2014). Therefore, the slopes of thin ridges tend to fail more easily and particularly when they are perpendicular to seismogenic faults due to tensile stress dominance.

To explore the topographic effects along seismogenic faults, the C-C' profile (Figure 2) was selected to perform a distribution analysis of landslides and topography. The landslide area and number of each band with 1.5 km width and 8 km length are illustrated in Figure 11. Band number starts from northwest to southeast. Band No.6, band No. 14~15, and band No. 17~18 represent the thin ridge near Jiuzhaitiantang, the Danzu valley, and the Rizhai valley, respectively. The topographic

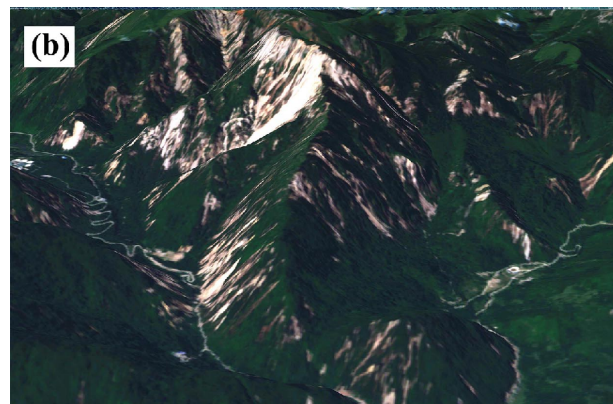
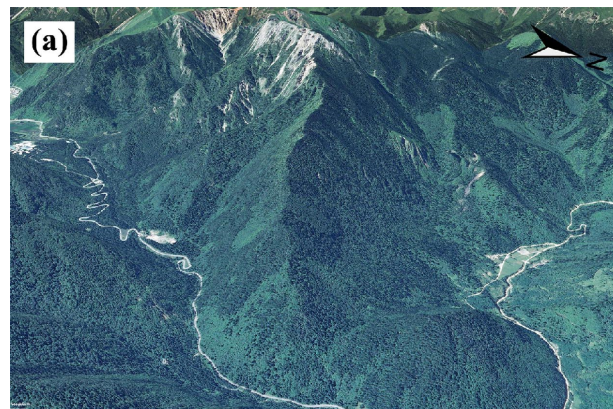


**Figure 10** Comparison of a thin ridge near Jiuzhaitiantang pre- and post-earthquake (enveloped by dash line in Figure 7a). (a) From Google Earth image (taken on 13th August 2013); (b) From Sentinel-2 image (downloaded from USGS <http://glovis.usgs.gov/>, and taken on 7th September 2017).

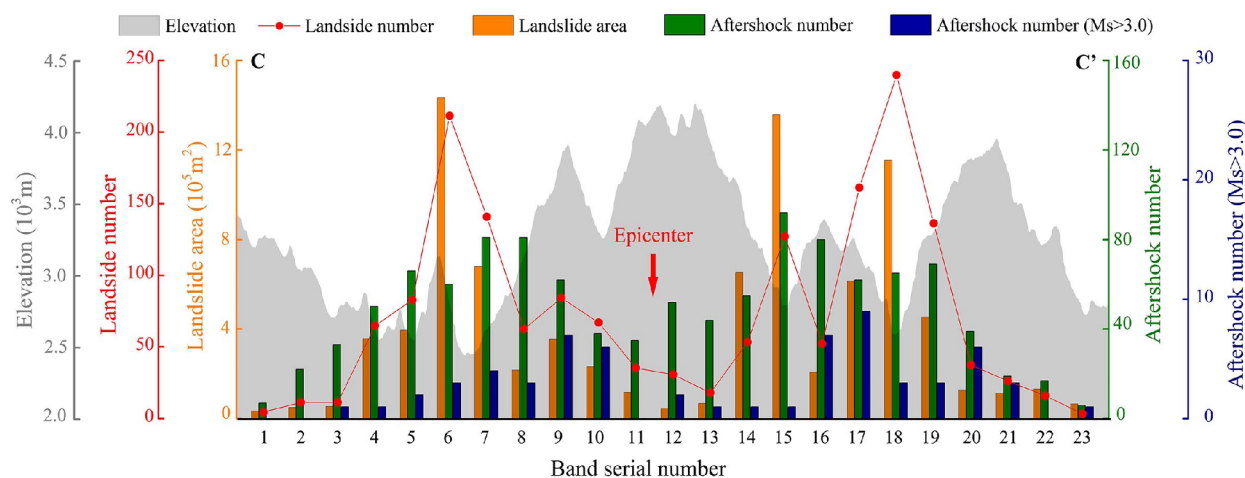


**Figure 11** Correlation between landslide density, aftershocks and topography of C-C' profile (Figure 2).

effects including back-slope direction and thin ridge amplification effects are clearly shown in Figure 11. The landslide areas and numbers of the three bands are greater than the others.

### 3.5 Synergetic effect of seismogenic faults and topography

As of 09:00 (Beijing time UTC+8) 18th August 2017, 5019 aftershocks had been recorded by CENC, including three aftershocks greater than  $M_s$  4.0. Aftershocks within the first 100 hours were generally located between the two blind strike-slip seismogenic faults (Figure 12). As seen in Figures 2 and 12, the spatial distribution of coseismic landslides and aftershocks shows great consistency. Their density is also similar and exhibits a bimodal distribution along the C-C' profile (Figure 11). These phenomena may be related to the rupturing processes. The strong shearing rupture

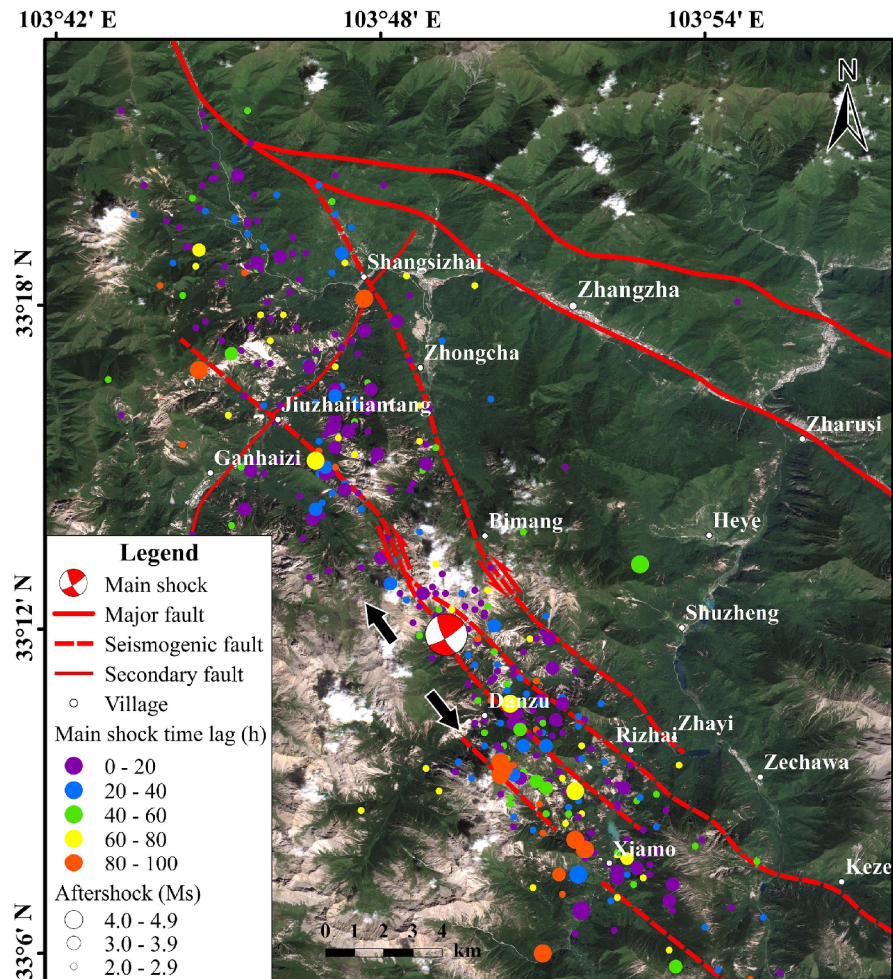


**Figure 12** Locations of aftershock ( $M_s$ >2.0) within the first 100 hours after the mainshock. Different colors show different time lag and different sizes of circles show different magnitudes of aftershocks. The black arrows represent rupture and aftershock propagating direction. The base map is a Sentinel-2 image downloaded from USGS (<http://glovis.usgs.gov/>).

propagated northwestward and southeastward simultaneously releasing energy along a narrow corridor. When the major rupture stopped propagating around Jiuzhaitiantang and Xiamo, the energy concentrated in the bidirectional ends of the seismogenic faults. The spatio-temporal distribution of aftershocks (Figures 11–12) and the latest source-process inversion result (Zhang et al. 2017) provide evidence for these hypothesis. The spatial pattern of 2017 Jiuzhaigou earthquake-triggered landslides can therefore be summarized as a synergetic effect of seismogenic faults and topography: (1) the earthquake energy concentrated within a narrow corridor determines the spatial distribution of the earthquake-triggered landslides; (2) earthquake energy aggregation in the bidirectional end of seismogenic faults and the topographic effects lead to distinct clusters of earthquake-triggered landslides.

#### 4 Discussion and Conclusion

The seismogenic fault geometry of this study was based on preliminary field investigations. Further understanding of the seismogenic faults and rupture processes will require additional data particularly high-resolution geophysical profiles. Lithology was not considered in this study. Most of the landslide areas occurred in limestone with a similar structure in most cases (Dai et al. 2017).

The 2017 Jiuzhaigou earthquake demonstrated that the seismogenic faults confine the general spatial pattern of coseismic landslides and local topography controls distinct clusters of slope failure. By using visual interpretation and field investigation, an inventory map integrated by 2212 earthquake-triggered landslides covering an area of approximately 11.8 km<sup>2</sup> was developed. Most landslides exhibited a close spatial correlation with seismogenic faults. More than 85% of the landslides occurred at elevations ranging from 2200 to 3700 m asl, but few landslides occurred above 3700 m asl. This finding deserves further investigation. Local topographic relief showed a stronger correlation in relation to other topographic factors for landslide distribution. The

study area is dominated by slopes ranging from 10°~40°, but slopes in 20°~50° were the most susceptible to landslides, as they account for 85.5% of the total number of coseismic landslides. Highest landslide density occurred on slopes with aspects nearly vertical to the orientation of the seismogenic fault slip. Additionally, the back-slope direction, thin-ridge amplification and synergetic effects of seismogenic faults and topography on the distribution of landslides triggered by this earthquake were satisfactorily demonstrated. It is hoped that the data and results of this study will lead toward a more comprehensive understanding of buried-rupture earthquake triggered landslides.

Given the impact of the Jiuzhaigou earthquake on the National Park, we agree with the argument provided by Alcántara-Ayala (2009) regarding the necessity to introduce disaster risk management strategies in geoparks, geomorphosites, national parks and all UNESCO World Heritage Sites to raise awareness and preparedness of visitors and inhabitants of the surrounding areas to prevent potential disasters.

#### Acknowledgement

This research was supported by the Key Laboratory Program for Mountain Hazards and Earth Surface Process, CAS (Grant No. KLMHESP-17-06), International Science Program-Silk Road Disaster Risk Reduction (Grant No. 131551KYSB20160002), Major International (Regional) Joint Research Project (Grant No. 41520104002), Key Research Program of Frontier Sciences, CAS (Grant No. QYZDY-SSW-DQC006), and 135 Strategic Program of the Institute of Mountain Hazards and Environment, CAS, NO. SDS-135-1701. We are grateful to FAN Xuanmei and XU Qiang from State key laboratory of Geohazard prevention and Geoenvironment Prevention for generously providing the interpretation landslide data. Deep appreciation goes to WANG Meimei and WU Shengnan for their helpful comments. We thank anonymous referees and editors for their constructive comments on an earlier version of this paper.

## References

- Alcántara-Ayala I (2009) Geomorphosite management in areas sensitive to natural hazards, In: Reynard E, Coratza P, Regolini-Bissing G (Eds), *Geomorphosites*, Pfeil Verlag, München. pp 163-173. ISBN 978-3-89937-094-2.
- Chen XZ, Cui YF (2017) The formation of the Wulipo landslide and the resulting debris flow in Duijiangyan City, China. *Journal of Mountain Science* 14(6): 1100-1112. <https://doi.org/10.1007/s11629-017-4392-1>
- Chen X, Zhou Q, Liu C (2015) Distribution pattern of coseismic landslides triggered by the 2014 Ludian, Yunnan, China Mw6.1 earthquake: special controlling conditions of local topography. *Landslides* 12(6):1159-1168. <https://doi.org/10.1007/s10346-015-0641-y>
- Chousianitis K, Del Gaudio V, Sabatakakis N, et al. (2016) Assessment of earthquake-induced landslide hazard in Greece: From Arias intensity to spatial distribution of slope resistance demand. *Bulletin of the Seismological Society of America* 106(1): 174-188. <https://doi.org/10.1785/0120150172>
- Chousianitis K, Del Gaudio V, Kalogeras I, et al. (2014) Predictive model of Arias intensity and Newmark displacement for regional scale evaluation of earthquake-induced landslide hazard in Greece. *Soil Dynamics and Earthquake Engineering* 65: 11-29. <https://doi.org/10.1016/j.soildyn.2014.05.009>
- Cui P, Liu SQ, Tang BX, et al. (2005) *Research and Prevention of Debris Flow in National Park*. Science press, Beijing, China. pp 90-91.
- Cui P, Xiang LZ, Zou Q (2013) Risk assessment of highways affected by debris flows in Wenchuan Earthquake area. *Journal of Mountain Sciences* 10(2): 173-189. <https://doi.org/10.1007/s11629-013-2575-y>
- Cui P, Zhang J, Yang Z, et al. (2014) Activity and distribution of geohazards induced by the Lushan earthquake, April 20, 2013. *Natural hazards* 73(2): 711-726. <https://doi.org/10.1007/s10669-014-1100-0>
- Cui YF, Chan D, Nouri A (2017) Coupling of solid deformation and pore pressure for undrained deformation—a discrete element method approach. *International Journal for Numerical & Analytical Methods in Geomechanics*, 41(1):1-19. <https://doi.org/10.1002/nag.2708>
- Cui YF, Zhou XJ, Guo CX (2017) Experimental study on the moving characteristics of fine grains in wide grading unconsolidated soil under heavy rainfall. *Journal of Mountain Science* 14 (3):417-431. <https://doi.org/10.1007/s11629-016-4303-x>
- Dai LX, Xu Q, Fan XM et al. (2017) A preliminary study on spatial distribution patterns of landslides triggered by Jiuzhaigou earthquake in Sichuan on August 8th, 2017 and their susceptibility assessment. *Journal of Engineering Geology* 25 (4): 1151-1164. (In Chinese) <https://doi.org/10.13544/j.cnki.jeg.2017.04.030>
- Davis LL, West LR (1973) Observed effects of topography on ground motion. *Bulletin of the Seismological Society of America* 63(1):283-298.
- Gorum T, Korup O, Westen CJV, et al. (2014) Why so few? Landslides triggered by the 2002 Denali earthquake, Alaska. *Quaternary Science Reviews* 95(7): 80-94. <https://doi.org/10.1016/j.quascirev.2014.04.032>
- Gorum T, Van Westen CJ, Korup O, et al. (2013) Complex rupture mechanism and topography control symmetry of mass-wasting pattern, 2010 Haiti earthquake. *Geomorphology* 184: 127-138. <https://doi.org/10.1016/j.geomorph.2012.11.027>
- Guzzetti F, Ardizzone F, Cardinali M, et al. (2009) Landslide volumes and landslide mobilization rates in Umbria, central Italy. *Earth & Planetary Science Letters* 279(3-4): 222-229. <https://doi.org/10.1016/j.epsl.2009.01.005>
- Harp EL, Wilson R C (1995) Shaking intensity thresholds for rock falls and slides: evidence from the whittier narrows and superstition hills earthquake strong motion records. *Bulletin of the Seismological Society of America* 85(6): 1739-1757.
- Harp EL, Jibson R W (2002) Anomalous concentrations of seismically triggered rock falls in pacoima canyon: are they caused by highly susceptible slopes or local amplification of seismic shaking? *Bulletin of the Seismological Society of America* 92(8): 3180-3189. <https://doi.org/10.1785/0120170033>
- Hayes GP, Briggs RW, Sladen A, et al. (2010) Complex rupture during the 12 January 2010 Haiti earthquake. *Nature Geoscience* 3(11): 800-805. <https://doi.org/10.1038/ngeo977>
- Hsieh SY, Lee CT (2011) Empirical estimation of the Newmark displacement from the Arias intensity and critical acceleration. *Engineering Geology* 122(1): 34-42. <https://doi.org/10.1016/j.enggeo.2010.12.006>
- Ji LY, Liu CJ, Xu J, et al. (2017) InSAR observation and inversion of the seismogenic fault for the 2017 Jiuzhaigou Ms7.0 earthquake in China. *Chinese Journal of Geophysics* (In Chinese), 60(10): 4069-4082, <https://doi.org/10.6038/cjg20171032>
- Kamp U, Growley B J, Khattak G A, et al. (2008) GIS-based landslide susceptibility mapping for the 2005 Kashmir earthquake region. *Geomorphology*: 101(4): 631-642. <https://doi.org/10.1016/j.geomorph.2008.03.003>
- Kargel JS, Leonard GJ, Shugar DH, et al. (2016) Geomorphic and geologic controls of geohazards induced by Nepal's 2015 Gorkha earthquake. *Science* 351(6269): aac8353. <https://doi.org/10.1126/science.aac8353>
- Kieffer DS, Jibson R, Rathje EM, et al. (2006) Landslides triggered by the 2004 Niigata Ken Chuetsu, Japan, earthquake. *Earthquake Spectra* 22(S1): 47-73. <https://doi.org/10.1193/1.2173021>
- Korup O, Clague JJ, Hermanns RL, et al. (2007) Giant landslides, topography, and erosion. *Earth & Planetary Science Letters* 261(3-4):578-589. <https://doi.org/10.1016/j.epsl.2007.07.025>
- Korup O, Montgomery DR, Hewitt K (2010) Glacier and landslide feedbacks to topographic relief in the Himalayan syntaxes. *Proceedings of the National Academy of Sciences of the United States of America* 107(12): 5317-22. <https://doi.org/10.1073/pnas.0907531107>
- Li YS, Huang C, Yi SJ, et al. (2017) Study on seismic fault and source rupture tectonic dynamic mechanism of Jiuzhaigou Ms 7.0 earthquake. *Journal of Engineering Geology* 25 (4): 1141-1150. (In Chinese) <https://doi.org/10.13544/j.cnki.jeg.2017.04.029>
- Luo Y, Gaudio VD, Huang R, et al. (2014) Evidence of hillslope directional amplification from accelerometer recordings at Qiaozhuang (Sichuan – China). *Engineering Geology*: 183:193-207. <https://doi.org/10.1016/j.enggeo.2014.10.015>
- Malamud BD, Turcotte DL, Guzzetti F, et al. (2010) Landslide inventories and their statistical properties. *Earth Surface Processes & Landforms*: 29(6):687-711. <https://doi.org/10.1002/esp.1064>
- Meunier P, Hovius N, Haines AJ (2007) Regional patterns of earthquake - triggered landslides and their relation to ground motion. *Geophysical Research Letters* 34(20): L20408. <https://doi.org/10.1029/2007GL031337>
- Meunier P, Uchida T, Hovius N (2013) Landslide patterns reveal the sources of large earthquakes. *Earth & Planetary Sciences Letters* 363(2): 27-33. <https://doi.org/10.1016/j.epsl.2012.12.018>
- Papathanassiou G, Valkaniotis S, Ganas A, et al. (2013) GIS-based statistical analysis of the spatial distribution of earthquake-induced landslides in the island of Lefkada, Ionian Islands, Greece. *Landslides*: 10(6):771-783. <https://doi.org/10.1007/s10346-012-0357-1>

- Pischutta M, Cultrera G, Caserta A, et al. (2010) Topographic effects on the hill of Nocera Umbra, central Italy. *Geophysical Journal International* 182(2): 977-987. <https://doi.org/10.1111/j.1365-246X.2010.04654.x>
- Poursartip B, Fathi A, Kallivokas LF. (2017) Seismic wave amplification by topographic features: A parametric study. *Soil Dynamics and Earthquake Engineering* 92: 503-527. <https://doi.org/10.1016/j.soildyn.2016.10.031>
- Ren JJ, Xu XW, Zhang SM, et al. (2017) Tectonic transformation at the eastern termination of the Eastern Kunlun fault zone and seismogenic mechanism of the 8 August 2017 Jiuzhaigou MS7.0 earthquake. *Chinese Journal of Geophysics*, 60(10): 4027-4045. (In Chinese) <https://doi.org/10.6038/cjg20171029>
- Stein RS, King GCP, Lin J (1994) Stress triggering of the 1994 M= 6.7 Northridge, California, earthquake by its predecessors. *Science*, 265(5177): 1432-1435. <https://doi.org/10.1126/science.265.5177.1432>
- Xu C, Xu X (2014) Statistical analysis of landslides caused by the Mw 6.9 Yushu, China, earthquake of April 14, 2010. *Natural Hazards*: 72(2):871-893. <https://doi.org/10.1007/s11069-014-1038-2>
- Xu C, Xu X, Shyu JBH, et al. (2014) Landslides triggered by the 22 July 2013 Minxian-Zhangxian, China, Mw 5.9 earthquake: Inventory compiling and spatial distribution analysis. *Journal of Asian Earth Sciences* 92(5): 125-142. <https://doi.org/10.1016/j.jseaes.2014.06.014>
- Xu Q, Zhang S, Li W (2011) Spatial distribution of large-scale landslides induced by the 5.12 Wenchuan earthquake. *Journal of Mountain Science*: 8(2): 246-260. <https://doi.org/10.1007/s11629-011-2105-8>
- Xu XW, Wen XZ, Han ZJ, et al. (2013) Lushan Ms 7.0 earthquake: A blind reserve-fault event. *Chinese Science Bulletin*, 58(28-29): 3437-3443. <https://doi.org/10.1007/s11434-013-5999-4>
- Xu XW, Chen GH, Wang QX et al. (2017) Discussion on seismogenic structure of Jiuzhaigou earthquake and its implication for current strain state in the southeastern Qinghai-Tibet Plateau. *Chinese Journal of Geophysics* 60(10): 4018-4026. (In Chinese) <https://doi.org/10.6038/cjg20171028>
- Yalcin A (2008) GIS-based landslide susceptibility mapping using analytical hierarchy process and bivariate statistics in Ardesen (Turkey): Comparisons of results and confirmations. *Catena*: 72(1):1-12. <https://doi.org/10.1016/j.catena.2007.01.003>
- Zhang X, Feng WP, Xu LS, et al. (2017) The source-process inversion and the intensity estimation of the 2017 MS7.0 Jiuzhaigou earthquake. *Chinese Journal of Geophysics* 60(10): 4105-4116. (In Chinese) <https://doi.org/10.6038/cjg20171035>
- Zhou S, Chen G, Fang L (2016) Distribution Pattern of Landslides Triggered by the 2014 Ludian Earthquake of China: Implications for Regional Threshold Topography and the Seismogenic Fault Identification. *ISPRS International Journal of Geo-Information* 5(4):46. <https://doi.org/10.3390/ijgi5040046>
- Zhou XT, Han JL, Shi FG et al. (2014) Numerical simulation for amplification effect of topography and geomorphology to seismic waves. *Journal of Engineering Geology* 22 (6): 1211-1220. (In Chinese) <https://doi.org/10.13544/j.cnki.jeg.2014.06.027>